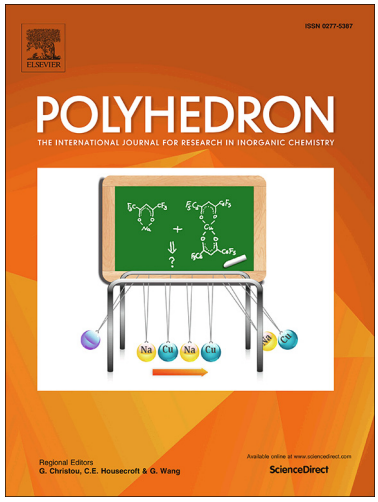

Titania surface chemistry and its influence on supported metal catalysts

Akbar Mahdavi-Shakib, Samra Husremovic, Sohee Ki, Jessica Glynn, Lauren Babb, Janine Sempel, Ioannis Stavrinoudis, Juan Manuel Arce Ramos, Ryan Nelson, Lars C. Grabow, Thomas J. Schwartz, Brian G. Frederick, Rachel Narehood Austin

PII: S0277-5387(19)30324-9
DOI: https://doi.org/10.1016/j.poly.2019.05.012
Reference: POLY 13937

To appear in: *Polyhedron*

Received Date: 15 March 2019
Accepted Date: 7 May 2019

Please cite this article as: A. Mahdavi-Shakib, S. Husremovic, S. Ki, J. Glynn, L. Babb, J. Sempel, I. Stavrinoudis, J.M.A. Ramos, R. Nelson, L.C. Grabow, T.J. Schwartz, B.G. Frederick, R.N. Austin, Titania surface chemistry and its influence on supported metal catalysts, *Polyhedron* (2019), doi: https://doi.org/10.1016/j.poly.2019.05.012

Titania surface chemistry and its influence on supported metal catalysts.

Akbar Mahdavi-Shakib[2], Samra Husremovic[1], Sohee Ki,[1] Jessica Glynn[1], Lauren Babb[1], Janine Sempel[1], Ioannis Stavrinoudis[1], Juan Manuel Arce Ramos[3], Ryan Nelson[4], Lars C. Grabow[3], Thomas J. Schwartz[5], Brian G. Frederick[2], Rachel Narehood Austin[1]

1. Department of Chemistry, Barnard College of Columbia University, 3009 Broadway, New York New York 10027 USA rna2113@columbia.edu
2. Department of Chemistry, University of Maine, Orono ME 04469
3. Department of Chemical and Biomolecular Engineering, University of Houston 4726 Calhoun Rd. Houston, TX 77204-4004
4. Department of Chemistry, Bowdoin College, 255 Main Street Brunswick ME 04011
5. Department of Chemical and Biomedical Engineering, University of Maine, Orono ME 04469

Abstract: This work characterized the surface chemistry of a number of different titania samples including four commercial anatase samples, an anatase sample that we synthesized, the pyrogenic titania samples P25 and P90, and a commercial rutile sample. X-ray photoelectron spectroscopy (XPS), inductively coupled plasma-optical emission spectroscopy (ICP-OES), and Diffuse Reflectance Infrared Fourier Transform Spectroscopy (DRIFTS), were used to identify surface species and surface contaminants that might interfere with the acid/base properties of the surface hydroxyls. All commercial anatase samples were contaminated by sulfur, which diminished their effectiveness as metal oxide supports for heterogeneous catalysis and has implications for their utility as photocatalysts. Hydrogen-bonded surface hydroxyls remained after calcination up to 400 ^{o}C for all anatase samples, in contrast to rutile and the pyrogenic titania materials P25 and P90, in

which they were eliminated. Ru(0) catalysts on titania without hydrogen-bonded surface hydroxyls showed enhanced C-O hydrogenolysis selectivity in the presence of water while Ru(0) catalysts on titania with hydrogen-bonded surface hydroxyls showed diminished selectivity in water, suggesting that surface hydrophilicity is important for this reaction. Heteroepitaxy between rutile RuO_2 and rutile TiO_2 is not essential for the creation of small evenly-spaced supported Ru(0) nanoparticles, which are important in many catalytic reactions.

Introduction:

Earth-abundant metal oxides play important roles in a wide variety of technologies.[1-2] They can serve as photocatalysts for organic chemical reactions,[3] water splitting,[4-5] or solar energy conversion[6]. They can be used for oxidation, dehydration, dehydrogenation, desulfurization, oxychlorination, C-O bond activation, and isomerization reactions,[7-8] as well as for sensor[9-10] and optoelectronic applications.[11] These oxides are also commonly used as a support for reduced metal catalysts.[7, 12] Transition metal oxides doped into metal hydrides can store hydrogen,[13] while other metal oxides act as key interfaces for biocompatible materials.[14] Mesoporous metal oxides can provide shape selectivity to the reactions they catalyze.[15] The surface chemistry of metal oxides affects how they function in many of these roles.[1, 7-8, 14] Increasingly, attention has focused on proton-coupled electron transfer to and from metal oxides, requiring a chemical link to the surface as redox chemistry occurs.[16] Passivation of metals by metal oxides is often critical to their function.[17-18]

TiO_2 is one of the most studied metal oxides because of its wide range of applications in photocatalysis[19], catalysis[20], solar cells[21], and biocompatible implants[22]. The counter ion of the titanium precursor, solvent, surfactant, and temperature all significantly impact the crystal structure,

electronic structure, and the surface chemistry of TiO_2.[23] Therefore, detailed physico-chemical characterization of these materials is necessary. Here, we have performed detailed physico-chemical characterization of the most commonly used commercial TiO_2 samples and explored some of the effects of these characterized properties.

We have shown that metal oxide-supported noble metal catalysts can be coupled with fast pyrolysis for the conversion of biomass to fuels,[24-32] which helps address the some of the problems associated with our reliance on fossil fuels.[33-34] Thermal conversion of lignocellulosic biomass into second generation biofuels using fast pyrolysis has been proposed[24-25, 29, 35-36] and evaluated[37-39] as a potentially economically viable route for the sustainable production of liquid fuels.[40-42] Our group and others have found that Ru supported on TiO_2 is a particularly effective catalyst for the deoxygenation of phenol, a model compound which serves to simplify the complexity of bio-oils.[43-45] DFT studies of the reaction mechanism show that an amphoteric support is required for the direct deoxygenation (DDO) of phenol to benzene, without hydrogenation of the ring.[43] In the proposed mechanism, the reaction is initiated by heterolytic dissociation of H_2 at the metal support interface. Heteroepitaxy between RuO_2, a common precursor in the synthesis of Ru/TiO_2 catalysts, and rutile TiO_2 is often invoked as a reason for the high activity of Ru/TiO_2 catalysts, although this effect has not been fully explored.[46-50] Our DFT calculations were performed on rutile (110) and experiments were performed on the Ru/P25 TiO_2, which contains anatase and rutile nanoparticles, leaving open questions about the role of crystal structure in catalysis.[43]

Given the importance of titania in a variety of catalytic applications, in this work we have characterized the surface chemistry of a number of different titania samples including four commercial anatase samples, an anatase sample that we synthesized, the pyrogenic titania samples P25 and P90, and a commercial rutile sample. We used X-ray photoelectron spectroscopy (XPS), inductively coupled plasma-optical emission spectroscopy (ICP-OES), and

Diffuse Reflectance Infrared Fourier Transform Spectroscopy (DRIFTS) to thoroughly characterize the metal oxide surfaces. DRIFTS measurements were also used to probe questions of surface hydrophobicity/hydrophilicity. Transmission electron microscopy (TEM) was used to show that all surfaces of titania can serve as nucleating agents for nanoparticulate Ru(0), thus ruling out an essential role for heteroepitaxy in creating these hybrid materials. These studies test hypotheses about why pyrogenic titania materials behave more like rutile than anatase despite being predominantly anatase, and our observations point to implications for catalytic reactions that utilize these materials.

Methods and Materials

Materials. Titanium dioxide P-25 (Evonik), Titanium dioxide P-90 (Evonik), TiO_2 rutile (US Research Nanomaterials), TiO_2 anatase (Sigma Aldrich, denoted "SA", US Research Nanomaterials, denoted "USR", Alfa Aesar, denoted "AA", Nanografi, denoted "NG") were all purchased from their respective manufacturers. Composition was confirmed by XRD (Fig S1). $RuCl_3 \cdot 3H_2O$, liquefied phenol, solid phenol, and diethyl ether were purchased from Sigma-Aldrich. 200 mesh Cu TEM grids and silicon nitride TEM grids were purchased from Ted Pella Inc. (Redding, CA).

Support treatment. To decrease the sulfur content of commercial anatase samples, selected anatase samples were calcined (5 h, 400 °C, O_2), reduced (5 h, 400 °C, H_2), and calcined (5 h, 400 °C, O_2) under flow conditions. These materials are indicated as "anatase_CRC" (anatase_calcined, reduced, calcined).

Anatase synthesis. Anatase was synthesized following a published procedure.[51] The resulting material, denoted "BC" (indicating the material was synthesized at Barnard College), has a surface area of 159 m^2/g, and a bimodal distribution of pores with maxima around 4 and 12 nm.

Catalyst Preparation. Catalysts were prepared on a 5 g scale with a metal loading of both 1 wt% and 2 wt% Ru. The metal precursor ($RuCl_3 \cdot 3H_2O$, 130 or 260 mg) was dissolved in Milli Q grade water (18 MΩ) and added to the support until a paste-like consistency was obtained. The mixture was dried overnight at 90 °C and crushed with a mortar and pestle to uniform consistency.

Catalyst Reduction. Catalysts were reduced immediately prior to each reaction in a 25 mL Parr 4590 microreactor sealed with a flat graphite gasket controlled by a Parr 4848 controller operated by SpecView. After sealing the catalyst in the reactor, the system was purged three times with Ar gas and gradually heated to 573 K under flowing H_2 gas. The reactor was kept under flowing H_2 for another 0.5 h at 573 K. Then, an additional 550 psig of H_2 was added and the system was maintained at that pressure and temperature for 1 h. The reactor was subsequently cooled to room temperature prior to venting the system.

Metal Determination. The wt% metal loading of the catalysts was determined using a Thermo Scientific iCAP 600 ICP-OES spectrometer with microwave-assisted digestion. Approximately 25 to 30 mg of catalyst was weighed and placed in a CEM EasyPrep microwave digestion vessel with 8 ml of a 3-to-1 mixture of HCl and HNO_3 (trace metal grade). The vessels were sealed and placed in a CEM MARS 6 microwave. The temperature was raised to 220 °C over two hours and then held for 30 min. The samples were cooled to room temperature before being diluted to a total volume of 50 ml in MilliQ water. The digested samples were analyzed by ICP and the ruthenium concentration was determined by comparing the emission to a calibration curve made using ruthenium standards with concentrations of 0 ppm, 4 ppm, and 12 ppm. Independent analysis of selected samples by Galbraith Laboratories confirmed these results.

Transmission Electron Microscopy (TEM). Conventional and high-resolution TEM was performed at Columbia University Nanoinitiative (CNI) electron microscopy facilities using an FEI Talos F200X transmission/scanning transmission microscope. The analyzed catalysts were mixed

with a minimal amount of 2-propanal and the mixture was suspended on either a lacey carbon film on a Cu grid or a silicon nitride membrane grid with a membrane thickness of 50 nm, frame thickness of 50 μm and nine 0.1 mm x 0.1 mm windows. The operating voltage of the FEI Talos was 200 kV. It was seen that prolonged exposure to the electron beam resulted in amorphization of the particles, and, therefore, in the results presented here, care was taken to minimize the imaging time. Additionally, it was found that the carbon layer in the holey carbon grids was not fully amorphous, making it difficult to unambiguously distinguish the particles from the supporting carbon layer. As a result, the silicon nitride membrane grids were used when there was a need for obtaining the clearest images of the particles.

XPS and BET analysis. TiO_2 samples were placed on carbon tape for XPS analysis. Samples were outgassed at room temperature and pressures < 10^{-8} torr for 3 h before the analyses. XPS analyses were performed using a SPECS PHOIBUS 100 MCD plus analyzer at a pass energy of 100 eV with an Al Kα X-ray source working at 240 W and 20 mA.

Nitrogen adsorption isotherms were measured at 77 K using a Micromeritics ASAP-2020 instrument. Samples were degassed at 350 °C for 4 h prior to the measurements. The pore size distributions were calculated using the BJH method,[52-53] and surface areas were calculated using the BET method.[54]

FTIR, DRIFTS analysis. DRIFT spectra were recorded using a Nicolet 6700 Fourier Transform Infrared (FTIR) spectrometer equipped with a Praying Mantis™ accessory (Harrick Scientific Production, IBC). KBr powder was placed in the sample cup inside a Harrick Scientific high temperature reaction chamber (HVC). The sample cup in the HVC was placed on a temperature-controlled sample stage equipped with a cartridge heater and a thermocouple. The sample cup temperature was controlled by a Harrick Scientific Automatic Temperature controller (ATC-024-1).

The TiO_2 samples were spread on top of the KBr powder in the sample cup for DRIFTS studies. After the material was loaded in the chamber, the environmental chamber was heated externally overnight with the sample maintained at 70 °C under an O_2 flow (Grade 2, Matheson). The O_2 was dried with a 13X molecular sieve trap (4 to 8 mesh, Acros Organics) immersed in a dry ice-acetone bath. Step-wise temperature-programmed calcination was performed in the environmental chamber while several DRIFTS spectra were recorded at each temperature. All the DRIFTS spectra were recorded under dry O_2 flow by accumulation of 512 scans at 8 cm^{-1} resolution using a DTGS detector. Single beam spectra measured after drying KBr at elevated temperatures were used for background correction of sample spectra at the corresponding temperatures.

Catalytic Reactions with Phenol. Following procedures used in prior published work[43, 55], 4 ml of liquefied phenol (~10 wt% water, Sigma Aldrich) was introduced into a 25 mL Parr reactor with 120 mg of catalyst reduced immediately prior to the reaction. The system was purged three times with Ar and pressurized to 5 psi under an Ar atmosphere. The temperature was then gradually increased to 573 K while stirring at 650 RPM. The autogenic pressure in the reactor was 50 psi after the set temperature was reached, at which point an additional 650 psi of H_2 was added to the system. Vapor-liquid equilibrium calculations indicate that most of the liquid in the reactor remains at this condition (see Supporting Information). The reaction time after final pressurization was 15 min. The system was repressurized if a 50 psi drop in pressure was observed. After the reaction, the system was rapidly cooled using an ice bath to prevent extended reaction times. Samples were immediately analyzed using GC/MS. The Weisz-Prater criterion was estimated to be 0.035 for the P25-supported catalyst (see Supporting Information), suggesting the reactions carried out here were performed in the absence of mass transfer limitations. Reactions without water were done as described above except 4.5 grams of solid phenol and 150 mg of catalyst were used. Control

experiments showed no reactivity of phenol in the absence of H_2 under these conditions. As a reference, reactions done with Ru/P25 with and without water yielded results identical to those previously reported.[43]

Gas Chromatography Mass Spectrometry (GC/MS). Two μL of the reaction mixture were diluted in 1.5 mL of diethyl ether. Samples were analyzed using an Agilent 7820GC System with a 7963 series autoinjector and 5977E network mass selective detector with a HP-5MS cross-linked 5% PH ME siloxane capillary column (dimensions of 30 m × 0.25 mm × 0.25 μm) using UHP He. The method consisted of a 2.2 min solvent delay, and a 5 min hold at 318 K, followed by a ramp at 10 K/min to 498 K. Product concentrations were obtained with reference to an external calibration curve. Selectivity was defined based on the relative amounts of products, according to Equation 1.

Equation 1 Definition of selectivity

$$Selectivity = \frac{C_{\text{Product},i}}{\sum_i C_{\text{Product},i}} \times 100\%$$

Results:

3.1 Surface chemistry determined by XPS

Pure anatase is commercially produced via the "sulfate method" while pyrogenic TiO_2 is produced from the gas-phase reaction of $TiCl_4$.[23, 56]. The presence of sulfate in commercial anatase samples is mentioned by several authors,[23, 57-58] but is most often neglected in the literature. In addition, sulfate is a common additive to TiO_2 to create Brønsted acidity[59] and to increase its photo-oxidation activity.[60-61] Therefore, it is necessary to elucidate the influence of sulfate on the surface chemistry of commercial anatase materials.

All of the TiO_2 samples studied in this work have been analyzed using XPS and ICP. SA, USR, AA, and NG anatase samples showed a S2p peak at 168.9 eV, characteristic of S^{6+}, not S^{2-} (Figure 1).[62] Consistent with the XPS results, ICP analysis also showed the presence of sulfate for SA, USR, AA, and NG anatase samples (Table 1). Since ICP is a bulk analysis method and XPS is a surface analysis method, the agreement between the sulfur contents measured by XPS and ICP indicates that the majority of the sulfate resides on the surface of the materials (see Section S.3 of the supplemental material).

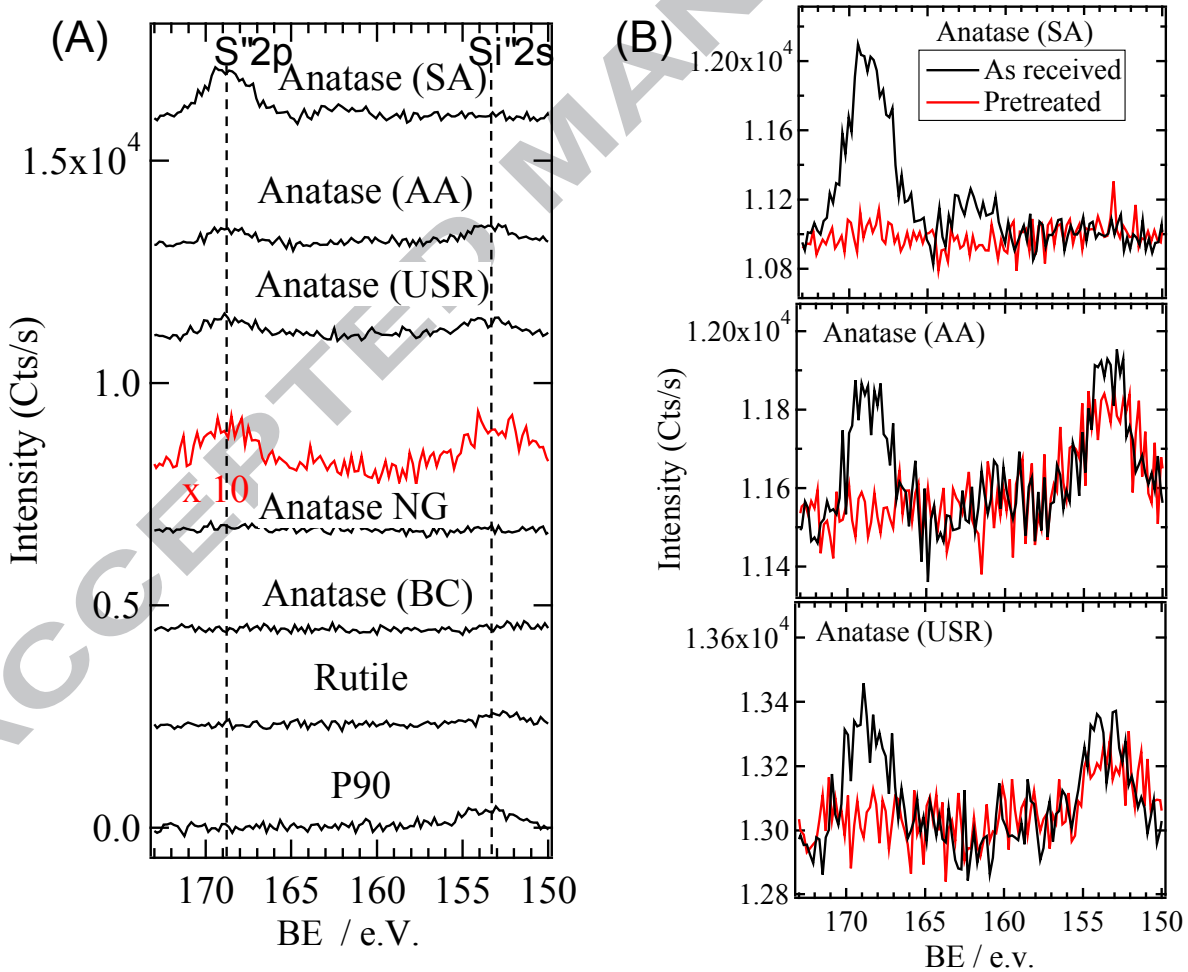

Figure 1. XPS analysis of the TiO_2 samples. A) XPS spectra of the as-received TiO_2 samples in the sulfur 2p and Si 2s region. The second (red) Anatase NG spectrum was multiplied by 10 due to the low intensity of the S signal, which was only visible with additional scans. Spectra are offset for clarity. Survey XPS scans are provided in the supplemental material and reveal Ti, O, and C peaks (Figure S2). B) XPS analysis of commercial anatase samples before (black spectra) and after 400°C calcination-reduction-calcination pretreatment (red spectra). These results showed that sulfate is eliminated after pretreatment at 400 °C.

The commercial anatase samples were subjected to a calcination/reduction/calcination cycle (each at 400 °C for 5 hr) in an attempt to decrease their sulfur content. The sulfur content decreased below the XPS (Figure 1B) and ICP-OES (Table 1) detection limits following this treatment. Additionally, to compare data to a sulfate-free anatase sample, anatase was synthesized at Barnard College from $TiCl_4$ as the titanium source. This anatase, labeled “anatase BC”, was free from sulfur as characterized by XPS (Figure 1A).

Table 1. Chemical and BET analysis of the TiO_2 samples

Material		S-content by XPS[a] (S atoms nm^{-2})	S-content by ICP-OES (ppm)	Surface area (m^2 g^{-1})
Pyrogenic	P90	ND[b]	<500	100
	P25	ND[b]	<500	55
Anatase	SA	1.5	3660	97
	SA_CRC	ND[b]	<500	NA[c]
	AA	0.5	1361	136

	AA_CRC	ND[b]	<500	NA[c]
	USR	0.5	782	97
	USR_CRC	ND[b]	<500	NA[c]
	NG	0.15	1310	280
	BC	ND[b]	NA[c]	159
Rutile	US research	ND[b]	<500	33

[a] Information on how the surface sulfur coverage was determined is provided in the supplemental information.

[b] None Detected

[c] Not Available

3.2 DRIFTS characterization of TiO_2 samples

FTIR spectroscopy provides a method for observing both surface sulfate species and surface hydroxyl groups and detecting perturbations to these key surface moieties that originate from the different TiO_2 sources. In addition, spectra recorded at different temperatures can guide the design of the pretreatment methods that remove sulfate.

DRIFTS spectra of P90 recorded during step-wise temperature-programmed calcination are shown in Figure 2A. The DRIFTS spectrum of the sample recorded at 30 °C shows several bands, indicating many chemical species are present on the surface at this temperature. The 1357, 1444, and 1547 cm^{-1} bands are assigned to the carbonate/bicarbonate species that are formed upon exposure of the surface to atmospheric CO_2.[63] The 1624 cm^{-1} band is assigned to the bending mode of physisorbed water. The broad absorbance feature in the 2500-3500 cm^{-1} region is assigned to hydrogen-bonded water and surface hydroxyls.[64-65] The bands in the 3600-3800 cm^{-1} region are from isolated surface hydroxyls and water molecules coordinated to surface Lewis acid

sites.[66] DRIFTS analysis of P90 shows that water is removed at 200 °C, carbonates at 300 °C, and isolated surface hydroxyls at 400 °C.

DRIFTS spectra of anatase AA are shown in Figure 2B. Similar to P90, water is eliminated at 200 °C and carbonates are eliminated at 300 °C. There is an additional band in this spectrum at 1311 cm^{-1} that continuously blue-shifts to 1358 cm^{-1} at 300 °C. This blue shift is indicative of surface sulfate species.[67] The sulfate band is eliminated after calcination at 400 °C. Similar spectral behavior was observed for other commercial anatase samples (see Figure 2C for anatase NG and Figures S3 and S4 for anatase USR and SA). Observation of the sulfate band in the spectra of these samples is consistent with the XPS and ICP data. Interestingly, the broad hydrogen-bonded hydroxyl absorbance feature in the 2500-3600 cm^{-1} range is not eliminated even after calcination at 400 °C. Anatase BC was synthesized following a sulfate-free method, and DRIFTS spectra of this sample show that water and carbonate are removed upon calcination at 300 °C; however, isolated and hydrogen-bonded surface hydroxyls are retained even after calcination at 400 °C (See Figure S5).

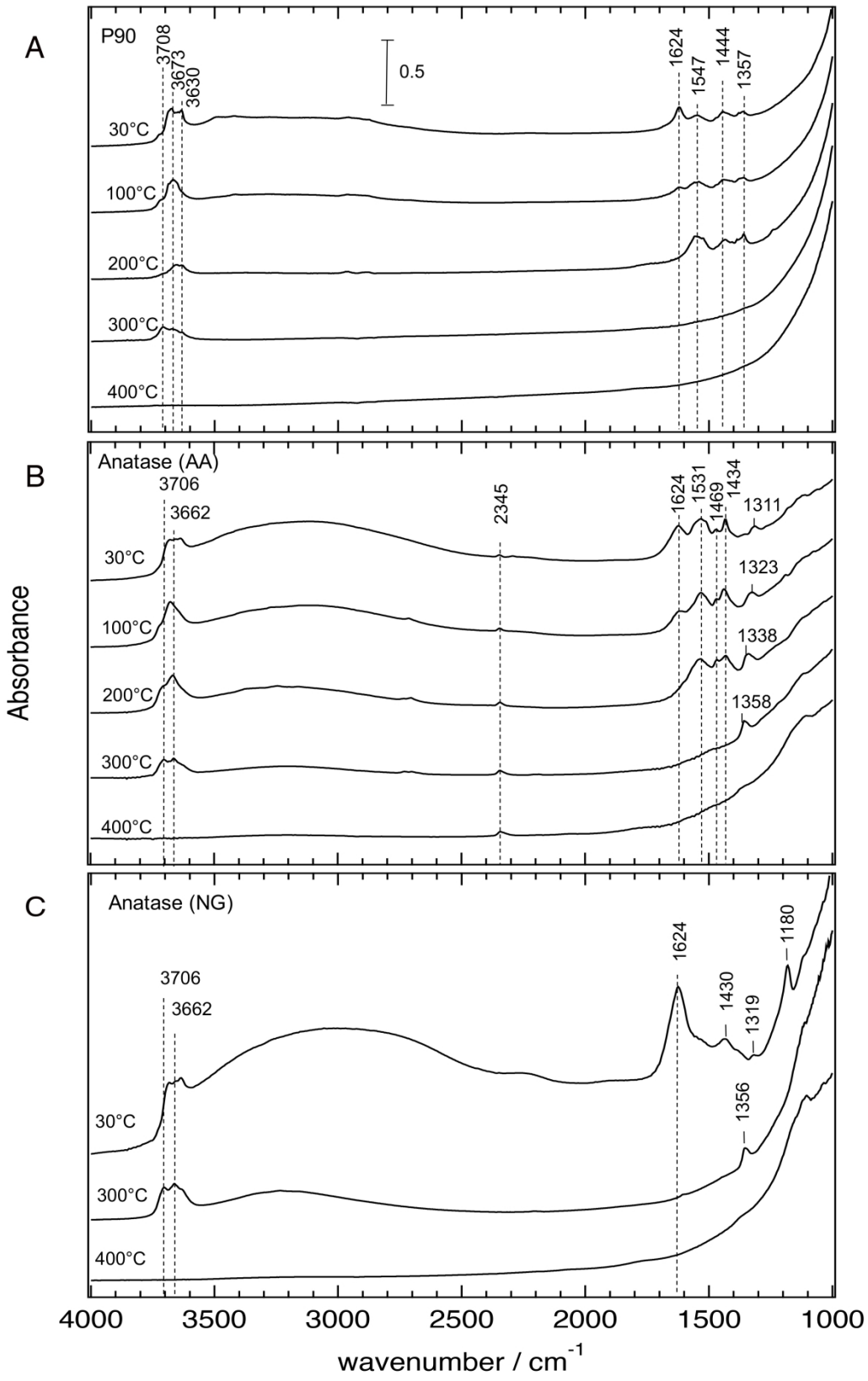
A
P90
3708
3673
3630
0.5
1624
1547
1444
1357
30°C
100°C
200°C
300°C
400°C
B
Anatase (AA)
3706
3662
2345
1624
1531
1469
1434
1311
1323
1338
1358
Absorbance
C
Anatase (NG)
3706
3662
1624
1430
1319
1180
1356
4000
3500
3000
2500
2000
1500
1000
wavenumber / cm-1

Figure 2. DRIFTS spectra of TiO_2 samples recorded during the calcination process from 30 °C to 400 °C. The band at 1180 cm^-1 in Figure 2C which gradually shifts to 1356 cm-1 upon heating is assigned S=O stretching of the sulfate groups.[67] The bands at 1357, 1444, and 1547 cm^{-1} are assigned to either surface carbonates or bicarbonate. [63, 68] The 1624 cm^{-1} band is assigned to the bending mode of water. The broad absorbance feature in the 2500-3600 cm^{-1} region contains the vibrational bands of water and H-bonded surface hydroxyls.[64-65] The bands in the 2800-3000 cm^{-1} region correspond to C-H stretching vibrations of hydrocarbon impurities. The complex absorbance features in the 3600-3800 cm^{-1} region are due to the vibrational modes of isolated hydroxyls.[66] Spectra are offset for clarity.

Surface hydroxyls are postulated as active sites for the DDO of phenol over Ru/TiO_2, and these species can be clearly observed in the spectra collected at 300 °C. Figure 3 shows three distinct bands at 3708 cm^{-1}, 3673 cm^{-1}, and 3630 cm^{-1} for the P90 and anatase BC. Observation of identical bands between anatase BC and P90 is consistent with P90 being 90% (w/w) anatase. In parallel work, we have assigned the FTIR absorbances that correspond to isolated surface hydroxyls on anatase nanopowders and used *ab initio* atomistic thermodynamics to define their thermodynamic stability under reaction conditions.[69] The 3708 cm^{-1} band is assigned to a terminal hydroxyl species on the anatase (001) surface and the 3673 cm^{-1} band is assigned to a bridging hydroxyl species on the anatase (101) surface.

We observed that the presence of surface sulfate species perturbs the surface hydroxyl bands. Anatase SA, which has the highest sulfate content, shows a featureless absorbance in this region. However, distinct features are observed for the other commercial anatase samples that all have lower sulfur contents (Table 1). The vibrational frequencies of the surface hydroxyl groups on the sulfated anatase are slightly different from those on the sulfate-free anatase; the 3708 cm^{-1}

band was red-shifted by approximately 2 cm^{-1} while the 3673 cm^{-1} band was red-shifted by 11 cm^{-1}. In addition to the frequency shift, the relative intensities also change in the presence of sulfate. The exact interpretation of these observations is outside the scope of this paper; however, they suggest that sulfate species may influence the acidity, basicity, and relative population of either the individual surface hydroxyls or the exposed crystal facets.

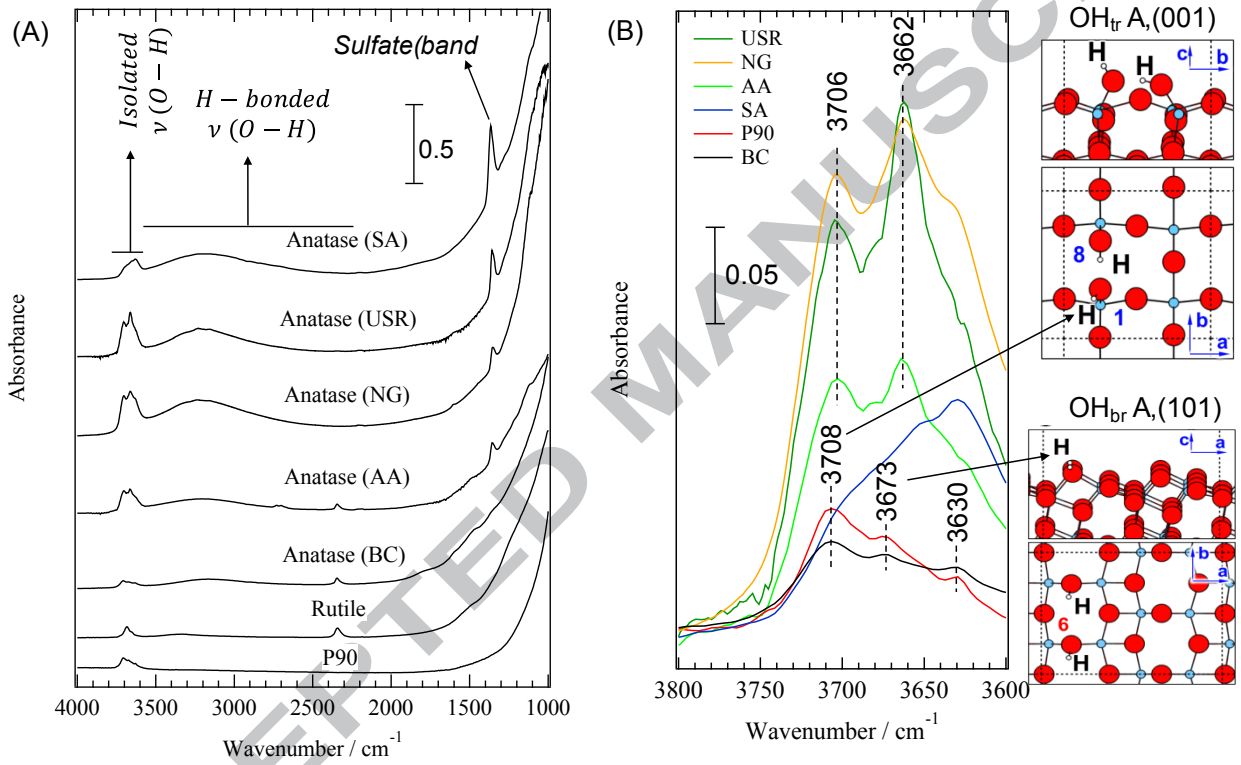

Figure 3. DRIFTS spectra of TiO_2 samples after overnight calcination at 300 °C. A) DRIFTS spectra in the 1000-4000 cm^{-1} range, spectra are offset for clarity B) isolated surface hydroxyl bands and the corresponding assignment of the 3708 cm^{-1} band to the hydrogen-bond receiving terminal hydroxyls of anatase (001) surface and the 3673 cm^{-1} band to the bridging hydroxyls of the anatase (101) surface.[69]

Another notable difference among the anatase samples was the broad absorbance feature observed in the 2500-3500 cm^{-1} region. Figure 4 shows the DRIFTS spectra for all the TiO_2 samples following overnight calcination at 400 °C. No bands were observed for the P90 sample, indicating the surface is completely dehydroxylated. In contrast, a broad absorbance from 2500-3500 cm^{-1} was observed for all the anatase samples, indicating that these samples are still partially hydroxylated and that these hydroxyl groups are in close enough proximity to participate in hydrogen bonding, consistent with the observations of Hadjiivanov et al.[23] Isotope exchange reactions with D_2O demonstrated that these hydroxyls are accessible and therefore excluded assignment to the OH stretch of trapped water molecules.[70]

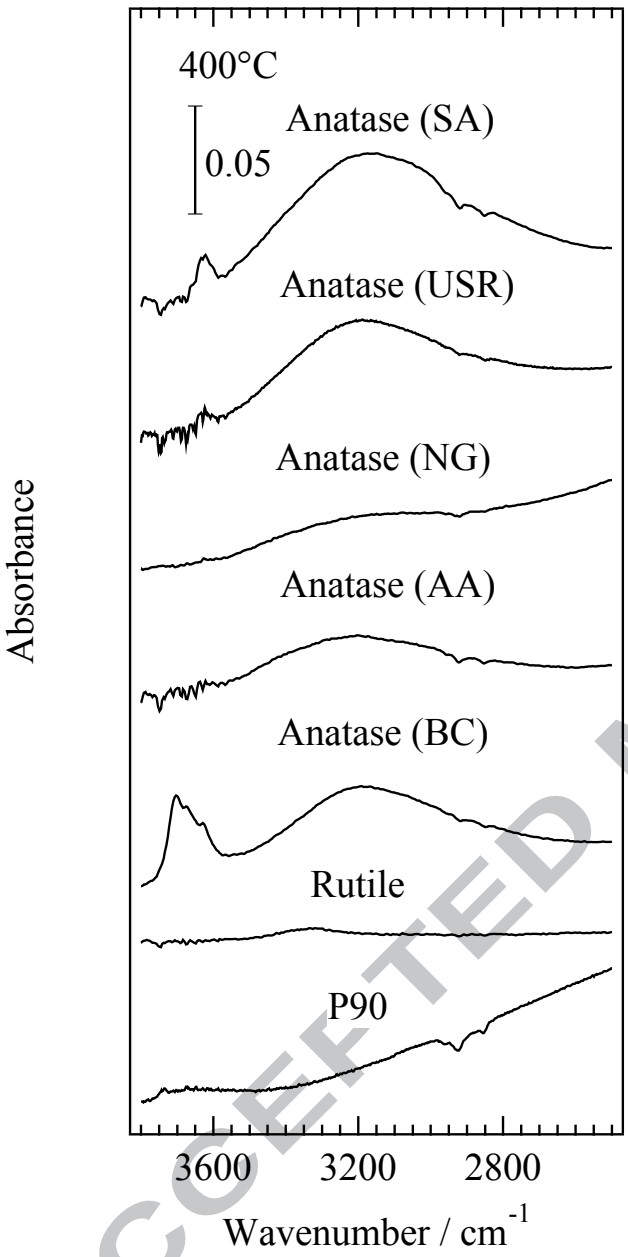

Figure 4. DRIFTS spectra of the P90, rutile, and anatase samples in the 2500-3800 cm^{-1} region after overnight calcination at 400°C. Spectra are offset for clarity.

3.3 TEM

Upon reduction in flowing hydrogen, Ru/TiO_2 catalysts form small evenly spaced nanoparticles of ruthenium, which are an essential component of selective HDO catalysts.[47, 55, 71-72] There are a number of questions about how nanoparticles form and what aspects of their structure are critical for reactivity. RuO_2 has a rutile crystal structure with lattice parameters well matched to those of rutile TiO_2, which has spawned speculation that heteroepitaxy between RuO_2 and rutile TiO_2 is important in nucleating Ru(0) nanoparticles.[49-50, 73-75] In our prior work, catalysts that had been calcined prior to reduction formed much larger, irregular ruthenium particles that preferentially catalyzed HYD reactions, which we attributed to the favorability of HYD on ruthenium.[55] In this work, TEM images of reduced Ru/rutile, Ru/anatase, Ru/P25, and Ru/P90 all show the presence of small Ru nanoparticles with an average particle diameter of 2 nm that did not vary significantly among supports (Figure 5 and Table 2). Prior work using CO chemisorption[55] to determine ruthenium particle size led to results consistent with particle diameters determined by TEM.

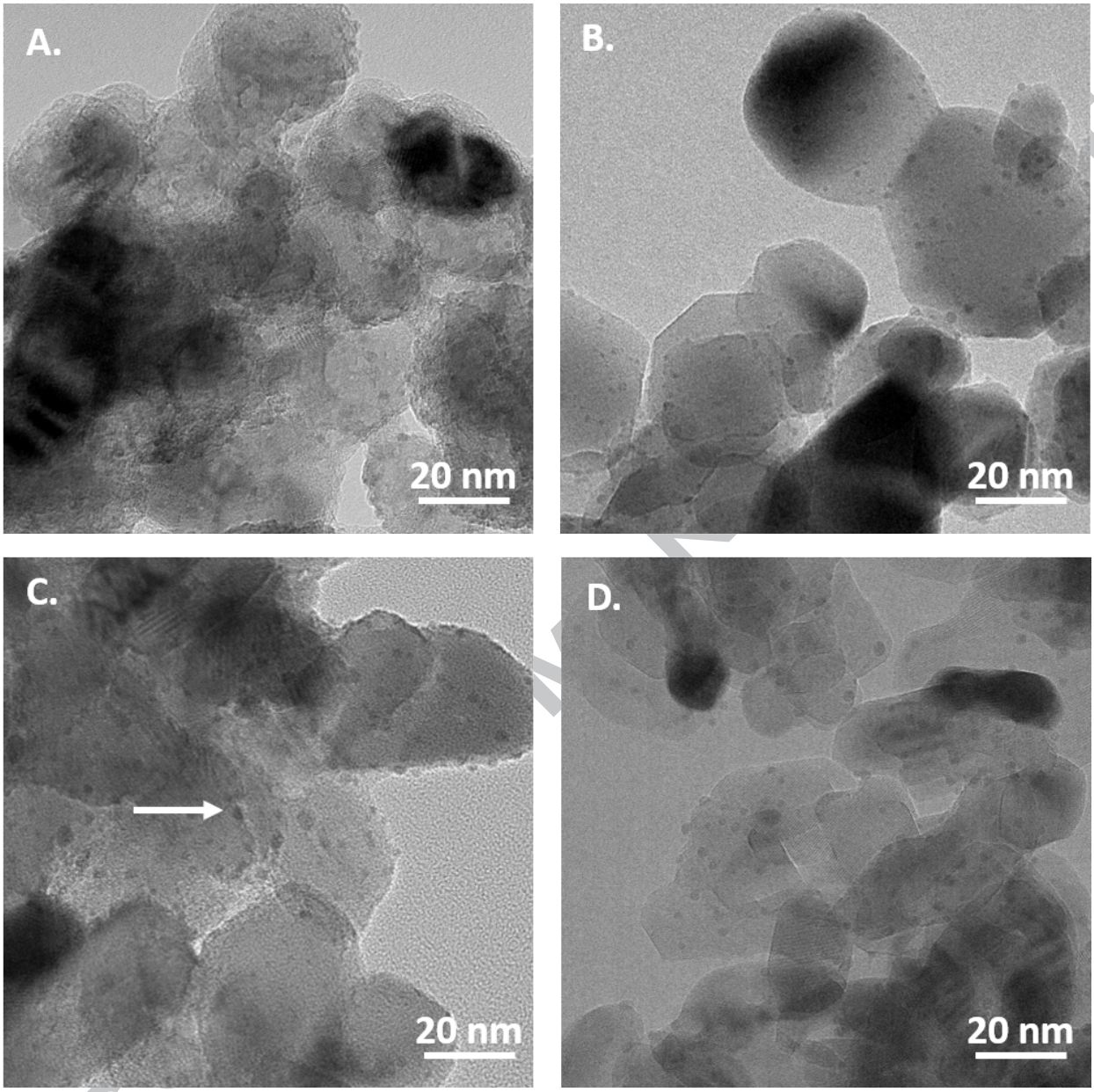

Figure 5 TEM images of active catalysts. Ru(0) nanoparticles are visible as darker spots against the lighter titania background. The white arrow points to one such Ru(0) nanoparticle. (A) Pretreated Ru on P90. (B) Pretreated Ru on P25 (C) Pretreated Ru on rutile (D) Pretreated Ru on anatase (Nanographi)

Support	Mean diameter (nm) and standard deviation
P90	1.7 +/- 0.5
P25	1.8 +/- 0.5
Anatase (SA and NG)	1.7 +/- 0.6
Rutile	2.0 +/- 0.5

Table 2: Mean diameter of ruthenium particles (nm) on TiO_2 supports as obtained from an analysis of TEM images. 200 particles from each material were measured.

3.4 Phenol deoxygenation reactions

We used the hydrodeoxygenation of phenol as a probe reaction to assess the catalytic activity of these materials (see Figure 6 for the reaction network). Ruthenium supported on Sigma Aldrich and Alfa Aesar anatase were not active for this reaction (phenol conversions less than 1%). The as-received anatase material from US Research achieved 6.5% phenol conversion. When this material was treated by calcining, reducing, and calcining to remove the sulfur, the phenol conversion increased to 22% at the same contact time. Nanographi anatase, which has very low sulfur content per surface area (0.14 S atoms per nm^2), was active as received.

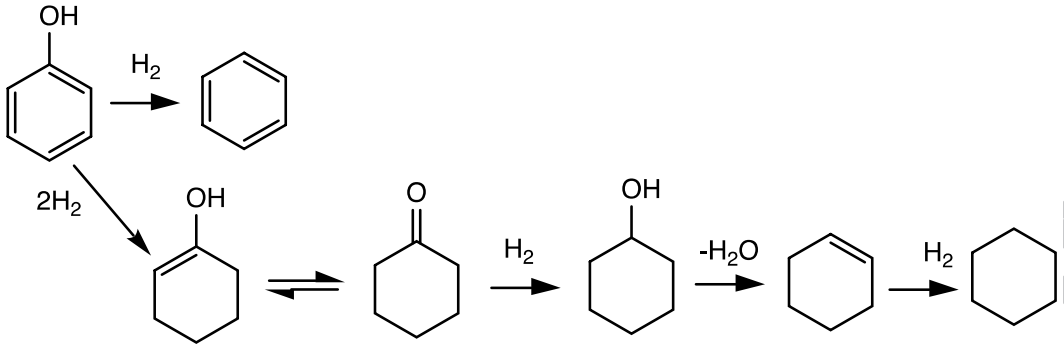

Figure 6 Reaction pathways for phenol in HDO catalysis. The top pathway, in which phenol is converted directly to benzene, is the direct deoxygenation pathway (DDO). The bottom pathway, in which phenol is sequentially hydrogenated, dehydrated, and hydrogenated, is the hydrogenation pathway (HYD).

We have previously shown that the reactivity of Ru/TiO_2 catalysts relies on a critical acid-base interaction at the interface between small nanoparticles of Ru and the amphoteric TiO_2 support (Figure 7).[43] Hydrogen adsorbs on the small Ru(0) particles, after which a basic surface hydroxyl facilitates H-H bond heterolysis. In a "rebound step", the protonated surface hydroxyl (now an acid), donates a proton to the phenolic oxygen, which weakens the C-O bond. C-O bond cleavage and hydride transfer complete the reaction cycle. Water favors the DDO pathway by increasing the surface concentration of protonated hydroxyls. Interestingly, the rutile-, P25-, and P90-supported catalysts all show an increase in DDO in the presence of water, whereas no increase was observed for the anatase-supported catalysts (Figure 8 and Table S1). This observation correlates with the greater stability of the hydrogen bonded surface hydroxyls in anatase as described above.

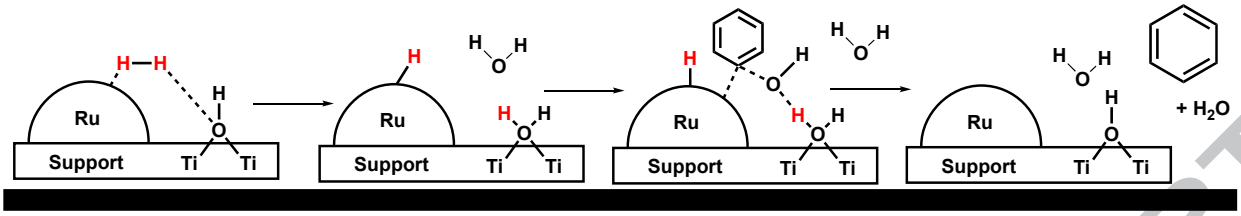

Figure 7 Reaction mechanism for selective DDO catalyst (adapted from 43). Surface hydroxyls facilitate heterolytic H-H bond cleavage and after being protonated serve as acids that donate a proton to the phenolic oxygen, weakening the C-O bond. Water suppresses desorption of the protonated hydroxyl, keeping the concentration of protonated surface hydroxyls relatively high.

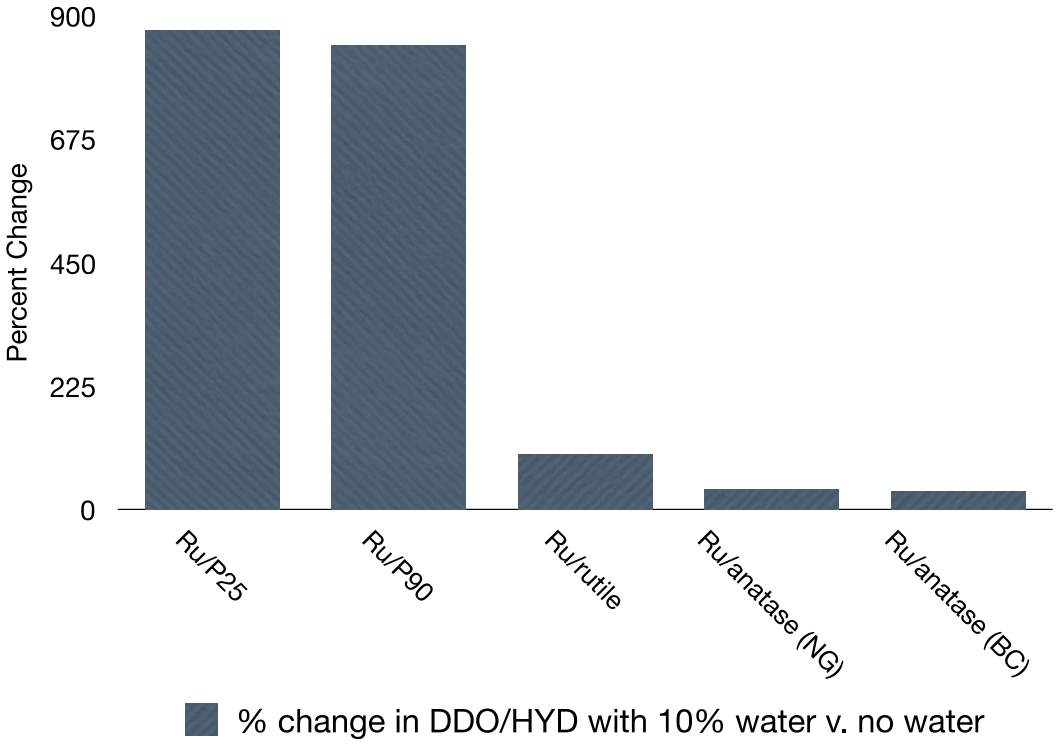

Figure 8. The role of water in influencing catalyst selectivity for the formation of benzene. The selectivity enhancement represents the percent change in the relative amount of benzene formed through the direct deoxygenation pathway to the relative amounts of all other products formed

through the hydrogenation pathway with and without the presence of 10 wt% water in the reaction for the same catalyst under comparable phenol conversions.

Discussion

In our earlier work, we demonstrated that small particles of Ru are required to achieve high selectivity for DDO, suggesting the active site for direct deoxygenation is at the interface between the particle and the support.[55] This model is consistent with recent work by Crossley et al. showing the rate of gas-phase DDO of cresol is proportional to the number of interfacial sites and specifically to the total perimeter length of the Ru-TiO_2 interface.[47, 71] We have also shown that water is a co-catalyst and provided a mechanistic explanation, based on DFT calculations, for its role.[43] Our earlier studies were performed using TiO_2 P25 as the support.

In this work, we observed that reactivity of the catalyst strongly depends on the support used. P90 and rutile are analogous to P25 in terms of DDO selectivity and response to water. The observation that all the commercial anatase materials we studied were contaminated by surface sulfate species explains the diminished catalytic activity we saw for untreated materials. We showed that sulfate impurities of commercial anatase samples could be removed after pretreatment at 400 °C. However, catalysts made from all non-pyrogenic anatase samples behave very differently from all other catalysts in terms of their DDO selectivity and response to water. It is surprising that P90 and P25 behave more like rutile than pure anatase although they are mostly anatase (P90 is 90% anatase and 10% rutile and P25 is 85% anatase and 15% rutile). Understanding the difference between pyrogenic TiO_2 and pure (non-pyrogenic) anatase TiO_2 was central to this study.

The rutile structure of RuO_2, which is a precursor in most Ru(0) nanoparticle syntheses, has lead to the hypothesis that rutile TiO_2 should be particularly good in supporting Ru(0) catalysts.[49-50, 73-75] The results from Crossley *et al*., in which deoxygenation of *m*-cresol is insensitive to TiO_2

crystal structure[71] while deoxygenation of guaiacol is not, provide no clear-cut answer to whether the structure of titania plays a role in DDO catalysts.[72] In this work we show that these small Ru(0) particles can form on any anatase crystal type, ruling out the hypothesis that there is some sort of epitaxial matching between rutile RuO_2 {110} and rutile TiO_2 {110} that either stabilizes the RuO_2 phase or facilitates high dispersion in the activated catalyst.

The FTIR characterization of these materials points to potential differences in the hydrophilicity of the titania surface, a phenomenon that is known to be important in certain applications. The DRIFT spectra of the low-temperature-synthesized and commercial anatase materials all show a broad hydrogen-bonded hydroxyl absorption that is not present in the spectra for pyrogenic TiO_2 after calcination above 200 ^oC. The absence of the 1620 cm^{-1} water-bending mode indicates that this band is not associated with chemisorbed or physisorbed water but is instead due to hydroxyls that are present in heterogeneous bonding conformations that hydrogen bond to nearby oxide oxygens. We have shown that these hydroxyls can be exchanged with D_2O, demonstrating that they are accessible surface hydroxyls.[70] Their persistence after calcination at 400 C indicates that their thermal stability is comparable or greater than the isolated hydroxyls, which we[69] and others[66] predict to be thermodynamically stable under reaction conditions.

Hadjiivanov in his 1996 review paper mentions that anatase samples undergo irreversible dehydroxylation upon when heated at up to 600 ^oC.[23] Pyrogenic TiO_2 is prepared at higher temperatures (between 1000 – 2400 ^oC), and under dry conditions, which explains why this material is less hydroxylated. Consequently, the low-temperature anatase surfaces should be much more hydrophilic than the pyrogenic anatase surface.

Water has been implicated in the catalytic activity of a number of titania-based heterogeneous catalysts. In the gas phase, Crossley and coworkers have shown that the DDO reaction rate increases in the presence of water, although the effect is negated when the amount of

water increases substantially relative to the number of Ru perimeter sites. They propose that water blocks active sites when present in quantities significantly in excess of the number of Ru perimeter sites, thereby leading to this decrease.[71] We suggest that this observation can also be rationalized based on density functional theory results presented in our previous work.[43] We showed that the presence of a water molecule increases the activation barrier for proton transfer from the Ru nanoparticle to the TiO_2 surface by 0.58 eV because H_3O^+-like transition states are less stable than H^+ transition states. Correspondingly, the DDO pathway requires heterolytic hydrogen cleavage across the Ru-TiO_2 interface to create the protonated hydroxyl site, which can proceed through an H^+-like or H_3O^+-like transition state. Similar conclusions regarding the detrimental effect of water on heterolytic H_2 activation across the Au/TiO_2 interface have been drawn from kinetic measurements, DFT calculations, and H-D exchange experiments.[76]

In the reactions carried out in the present study, the hydrophilic nature of the low-temperature anatase surfaces may lead to locally-enhanced water concentrations in the vicinity of the Ru perimeter sites, which in turn would lead to a higher barrier for regenerating the active site for DDO and the correspondingly-observed reduction in DDO rates. Kinetic water uptake measurements by Faria and coworkers indicate that the rate of water uptake on anatase is much more rapid than that on rutile, confirming the more hydrophilic nature of anatase surfaces.[74] Similarly, Stone and coworkers performed microcalorimetry measurements of water adsorption on anatase and rutile powders that indicate water adsorbs more strongly on anatase surfaces (heat of reversible adsorption = -60 kJ mol^{-1}) than on rutile surfaces (heat of reversible adsorption = -44 kJ mol^{-1})[77]. Thus, it is reasonable to assume that the surface concentration of water will be higher for anatase-supported catalysts than for rutile-supported catalysts, leading to depressed rates of heterolytic hydrogen cleavage. Conversely, the stronger heat of adsorption of water on anatase surfaces could lead to additional site-blocking by water for these systems. Both explanations are

consistent with our reactivity observations, and additional work is needed to discriminate between them.

The unique reactivity of Ru supported on pyrogenic TiO_2 could similarly be due to locally-manipulated water concentrations. While pyrogenic TiO_2 is mostly composed of anatase, it is mixed at the nanoscale with rutile crystallites. The hydrophobic nature of these crystallites may be sufficient to disrupt hydrogen-bonding networks of water distributed around the Ru nanoparticles, thereby decreasing the local concentration of water in P25- and P90-supported materials and leading to reactivity that is closer to rutile-supported catalysts than anatase-supported catalysts. Notably, the kinetic water uptake measurements from Faria's group show that the rates of water uptake on P25 lie between those for anatase and rutile,[74] supporting the notion that the nanoscale incorporation of rutile domains should lead to different amounts of water present near the Ru nanoparticles in our catalysts. While this hypothesis is consistent with the reactivity and characterization data presented here, additional work is needed to test it. Ultimately water could activate and/or deactivate either of the two competing pathways (HYD and DDO) that occur in these catalyst reactions.[78] Further studies to explore, in detail, the mechanistic role of water as a function of surface chemistry and morphology are underway.

Conclusion

This work focused on characterizing the surfaces of titania and three important ways in which they do and do not support catalytically-active nanoparticulate Ru(0)-based materials. We examined the presence of surface sulfur on a number of different titania materials and the influence this sulfur has on surface hydroxyls. We examined the presence of hydrogen bonded surface hydroxyls on titania, which is indicative of surface hydrophobicity/hydrophilicity. We studied whether the crystal structure impacts the ability of titania to support Ru(0) nanoparticles. The results of these investigations have implications for our catalytic work, but also for the work of

many other research efforts that use titania for the range of uses outlined in the introduction.

In this work, we show that commercial anatase samples contain varying amounts of sulfur on the surface and that this sulfur shifts hydroxyl stretching frequencies and diminishes catalytic activity in the phenol conversion reaction studied. We also show that all low-temperature synthesized anatase samples, regardless of sulfur content, contain thermally stable hydrogen-bonded surface hydroxyls that appear to foster a more hydrophilic surface than pyrogenic titania or rutile surfaces, in which these hydrogen-bonded surface hydroxyls do not form. Finally, all titania materials studied can nucleate the small Ru(0) nanoparticles that are important in a number of Ru(0)-based heterogeneous catalysts, ruling out an essential role for heteroepitaxy matching between rutile RuO_2 and rutile TiO_2 in their formation. Additional questions, however, about the role of electron transfer between the reducible metal oxide support and metal nanoparticle and the influence of water on the kinetic paramters of DDO v. HYD reactions[78], are not addressed by the characterizations provided here and will be the subject of further study.

Acknowledgements:

This work was supported by the U.S. National Science Foundation under award number NSF 1565843. SH was the recipient of two Hoffman grants from Bates College. We thank Simon Billinge, Katayun Barmak, Soham Banerjee, Daniela Stuck, and Amirali Zangiabadi for helpful discussions and Amiralia Zangiabadi for assistance with TEM imaging. We thank George Bernhardt for assistance in measuring XPS data.

Declaration of Interest: none

1. Fierro, J. L. G., Preface. In *Metal oxides: Chemistry and Applications*, Fierro, J. L. G., Ed. Taylor and Francis: 2006; p xi.
2. Wu, Y.; van Ree, T., 1 - Introduction: Energy technologies and their role in our life. In *Metal Oxides in Energy Technologies*, Wu, Y., Ed. Elsevier: 2018; pp 1-16.
3. Stone, V. F. J.; Davis, R. J., Syntheis, characterization, and photocatalytic activity of titania and niobia mesoporous molecular sieves. *Chem. Mater.* **1998,** *10*, 1468-1474.
4. Zong, X.; Li, C., 7 - Photocatalytic water splitting on metal oxide-based semiconductor photocatalysts. In *Metal Oxides in Heterogeneous Catalysis*, Védrine, J. C., Ed. Elsevier: 2018; pp 355-399.
5. Wang, J.; van Ree, T.; Wu, Y.; Zhang, P.; Gao, L., 8 - Metal oxide semiconductors for solar water splitting. In *Metal Oxides in Energy Technologies*, Wu, Y., Ed. Elsevier: 2018; pp 205-249.
6. Yuan, X.; Wu, X.; Wang, J.; Wu, Y.; van Ree, T., 12 - Solar-driven fuel production by metal-oxide thermochemical cycles. In *Metal Oxides in Energy Technologies*, Wu, Y., Ed. Elsevier: 2018; pp 321-340.
7. Védrine, J. C., 1 - Fundamentals of heterogeneous catalysis. In *Metal Oxides in Heterogeneous Catalysis*, Védrine, J. C., Ed. Elsevier: 2018; pp 1-41.
8. Goulas, K. A.; Mironenko, A. V.; Jenness, G. R.; Mazal, T.; Vlachos, D. G., Fundamentals of C–O bond activation on metal oxide catalysts. *Nature Catalysis* **2019**.
9. Wetchakun, K.; Samerjai, T.; Tamaekong, N.; Liewhiran, C.; Siriwong, C.; Kruefu, V.; Wisitsoraat, A.; Tuantranont, A.; Phanichphant, S., Semiconducting metal oxides as sensors for environmentally hazardous gases. *Sensors and Actuators B: Chemical* **2011,** *160* (1), 580-591.
10. Tiemann, M., Porous Metal Oxides as Gas Sensors. *Chemistry – A European Journal* **2007,** *13* (30), 8376-8388.
11. Yu, X.; Marks, T. J.; Facchetti, A., Metal oxides for optoelectronic applications. *Nature Materials* **2016,** *15*, 383-396.
12. 8 - Main industrial processes using metal oxides as catalysts or support and future trends in heterogeneous catalysis. In *Metal Oxides in Heterogeneous Catalysis*, Védrine, J. C., Ed. Elsevier: 2018; pp 401-549.
13. Chen, B.; Liu, Z.; Li, C.; Zhu, Y.; Fu, L.; Wu, Y.; van Ree, T., 9 - Metal oxides for hydrogen storage. In *Metal Oxides in Energy Technologies*, Wu, Y., Ed. Elsevier: 2018; pp 251-274.
14. Silva-Bermudez, P. r. n. R. M. r. n. R. S. E., The atomic ordering and its correlation to protein adsorption on biocompatible metal oxide coatings. *Frontiers in Bioengineering and Biotechnology*.
15. Ren, Y.; Ma, Z.; Bruce, P. G., Ordered mesoporous metal oxides: synthesis and applications. *Chemical Society Reviews* **2012,** *41* (14), 4909-4927.
16. Damatov, D.; Laga, S. M.; Mader, E. A.; Peng, J.; Agarwal, R. G.; Mayer, J. M., Redox reactivity of collodal nanoceria and use of optical spectra as an in situ monitor of Ce oxidation states. *Inorganic Chemistry* **2018,** *57*, 14401-14408.

17. Saji, V. S.; Choe, H. C.; Brantley, W. A., An electrochemical study on self-ordered nanoporous and nanotubular oxide on Ti–35Nb–5Ta–7Zr alloy for biomedical applications. *Acta Biomaterialia* **2009,** *5* (6), 2303-2310.
18. Asserghine, A.; Filotás, D.; Nagy, L.; Nagy, G., Scanning electrochemical microscopy investigation of the rate of formation of a passivating TiO2 layer on a Ti G4 dental implant. *Electrochemistry Communications* **2017,** *83*, 33-35.
19. Ohtani, B., design and Development of Active Titania and Related Photocatalysts. In *Photocatalysis and Water Purification: From Fundamentals to Recent Applications*, Pichat, P., Ed. Wiley-VCH: 2013; pp 74-102.
20. Centi, G.; Perathoner, S., Nano-architecture and reactivity of Titania catalytic materials. Quasi-1D nanostructures. *Catalysis* **2007,** *20*, 367-402.
21. Singh, R.; Dutta, S., A review on H2 production through photocatalytic reactions using TiO2/TiO2-assisted catalysts. *Fuel* **2018,** *220*, 607-620.
22. Liu, K.; Cao, M.; Fujishima, A.; Jiang, L., Bio-Inspired Titanium Dioxide Materials with Special Wettability and Their Applications. *Chemical Reviews* **2014,** *114* (19), 10044-10094.
23. Hadjiivanov, K.; Klissurski, D. G., Surface Chemistry of Titania (Anatase) and Titania-supported Catalysts. *Chem. Soc. Rev.* **1996,** *107*, 534-545.
24. Bridgwater, A. V., Renewable fuels and chemicals by thermal processing of biomass. *Chemical Engineering Journal* **2003,** *91*, 87-102.
25. Elliott, D. C., Historical Developments in Hydroprocessing Bio-oils. *Energy & Fuels* **2007,** *21*, 1792-1815.
26. Bridgwater, A. V.; Cottam, M.-L., Opportunities for Biomass Pyrolysis Liquids Production and Upgrading. *Energy & Fuels* **1992,** *6* (2), 113-120.
27. Bridgwater, A. V.; Double, J. M., A strategic assessment of liquid fuels from biomass. In *Research in Thermochemical Biomass Conversion*, Bridgwater, A. V.; Kuester, J. L., Eds. Elsevier Applied Science: New York, 1988; pp 98-110.
28. Garcia-Perez, M.; Chaala, A.; Pakdel, H.; Kretschmer, D.; Roy, C., Characterizaton of bio-oils in chemical families. *Biomass Bioenergy* **2007,** *31*, 222-242.
29. Huber, G. W.; Iborra, S.; Corma, A., Synthesis of Transportation Fuels from Biomass: Chemistry, Catalysts, and Engineering. *Chem. Rev.* **2006,** *106*, 4044-4098.
30. Ingram, L.; Mohan, D.; Bricka, M.; Steele, P.; Strobel, D.; Crocker, D.; Mitchell, B.; Mohammad, J.; Cantrell, K.; Pittman, C. U., Pyrolysis of wood and bark in an auger reactor: Physical properties and chemical analysis of the produced bio-oils. *Energy & Fuels* **2008,** *22* (1), 614-625.
31. Mullen, C. A.; Strahan, G. D.; Boateng, A. A., Characterization of Various Fast-Pyrolysis Bio-Oils by NMR Spectroscopy. *Energy & Fuels* **2009,** *23* (5), 2707-2718.
32. Oasmaa, A.; Meier, D., Characterisation, Analysis, Norms & Standards. In *Fast Pyrolysis of Biomass: A Handbook* Bridgwater, A. V., Ed. CPL Press: Newbury, UK, 2005; Vol. 3, pp 19-59.
33. Nashawi, I. S.; Malallah, A.; Al-Bisharah, M., Forecasting World Crude Oil Production Using Multicyclic Hubbert Model. *Energy Fuels* **2010,** *24*, 1788-1800.
34. Hemminger, J. C., Science for Energy Technology: Strengthening the link between Basic Research and Industry. *A report of a subcommittee to the Basic Energy Sciences Advisory Committee* **2010**.
35. Huber, G. W., Breaking the Chemical and Engineering Barriers to Lignocellulosic Biofuels: Next Generation Hydrocarbon Biorefineries. National Science Foundation. Chemical, B., Environmental, and Transport Systems Division, Ed. NSF: Washington, D.C., 2008.

36. Mortensen, P. M.; Grunwaldt, J.-D.; Jensen, P. A.; Knudsen, K. G.; Jensen, A. D., A review of catalytic upgrading of bio-oil to engine fuels. *Appl. Catal., A* **2011,** *407*, 1-19.
37. Ringer, M.; Putsche, V.; Scahill, J., Large-Scale Pyrolysis Oil Production: A Technology Assessment and Economic Analysis. 2006.
38. Wright, M. M.; Daugaard, D. E.; Satrio, J. A.; Brown, R. C., Techno-economic analysis of biomass fast pyrolysis to transportation fuels. *Fuel* **2010,** *89* (Suppl. 1), S2-S10.
39. Hayes, D. J., An examination of biorefining processes, catalysts and challenges. *Catalysis Today* **2009,** *145*, 138-151.
40. Perlack, R. D., Biomass as Feedstock for a Bioenergy and Bioproducts Industry: The Technical Feasibility of a Billion-Ton Annual Supply. DOE, Ed. Oak Ridge, TN, 2005; pp DOE/GO-102005-2135.
41. Dickerson, K.; Rubin, J.; J., K. *Biomass and Biofuels in Maine: Estimating Supplies for Expanding the Forest Products Industry*; Margaret Chase Smith Policy Center, Forest Bioproducts Research Intiative, Univ. of Maine: 2007.
42. Perlack, R. D.; Stokes, B. J. *U.S. Billion-Ton Update: Biomass Supply for a Bioenergy and Bioproducts Industry*; Oak Ridge, TN., 2011.
43. Nelson, R.; Baek, B.; Ruiz, P.; Goundie, B.; Brooks, A.; Wheeler, M. C.; Frederick, B. G.; Grabow, L. C.; Austin, R. N., Experimental and theoretical insights into the hydrogen-efficient direct hydrodeoxygenation mechanism of phenol over Ru/TiO_2. *ACS Catal.* **2015,** *11*, 6509-6523.
44. Wildschut, J.; Mahfud, F. H.; Venderbosch, R. H.; Heeres, H. J., Hydrotreatment of fast pyrolysis oil using heterogeneous noble-metal catalysts. *Ind. Eng. Chem. Res.* **2009,** *48*, 10324-10334.
45. Wildschut, J.; Melian-Cabrera, I.; Heeres, H. J., Catalyst studies on the hydrotreatment of fast pyrolysis oil. *Appl. Catal., B* **2010,** *99*, 298-306.
46. Carballo, J. M. G.; Finocchio, E.; Garcia, S.; Rojas, S.; Ojeda, M.; Busca, G.; Fierro, J. L. G., Support effects on the structure and performance of ruthenium catalysts for the Fischer-Tropsch synthesis. *Catal. Sci. Technol.* **2011,** *1*, 1013-1023.
47. Omotoso, T.; Boonyasuwat, S.; Crossley, S. P., Understanding the role of TiO_2 crystal structure on the enhanced activity and stability of Ru/TiO_2 catalysts for the conversion of lignin-derived oxygenates. *Green Chem.* **2014,** *16*, 645-655.
48. Pham, T. T.; Lobban, L. L.; Resasco, D. E.; Mallinson, R. G., Hydrogenation and Hydrodeoxygenation of 2-methyl-2-pentenal on supported metal catalysts. *J. Catal.* **2009,** *266* (1), 9-14.
49. Xiang, G.; Shi, X.; Wu, Y.; Zhuang, J.; Wang, X., Size effects in Atomic-Level Epitaxial Redistribution Process of RuO_2 over TiO_2. *Scientific Reports* **2012,** *2*, 801.
50. Kim, A.; Sanchez, C.; Patriarche, G.; Ersen, O.; Moldovan, S.; Wisnet, A.; Sassoye, C.; Debecker, D. P., Selective CO_2 methanation on Ru/TiO_2 catalysts: unravelling the decisive role of the TiO_2 support crystal structure. *Catal. Sci. Technol.* **2016,** *6*, 8117-8128.
51. Li, G.; Li, L.; Boerio-Goates, J.; Woodfield, B. F., High Purity Anatase TiO_2 Nanocrystals: Near Room-Temperature Synthesis, Grain Growth Kinetics, and Surface Hydration Chemistry. *J. Am. Chem. Soc* **2005,** *127*, 8659-8666.
52. Barrett, E. P.; Joyner, L. G.; Halenda, P. P., The Determination of Pore Volume and Area Distributions in Porous Substances. I. Computations from Nitrogen Isotherms. *J. Am. Chem. Soc* **1951,** *73*, 373-380.
53. Kruk, M.; Jaroniec, M.; Sayari, A., Application of Large-Pore MCM-41 Molecular Sieves to Improve Pore Size Analysis Using Nitrogen Adsorption Measurements. *Langmuir* **1997,** *13*.
54. Brunauer, S.; Emmett, P. H.; Teller, E., Adsoprtion of Gases in Multimolecular Layers. *J. Am. Chem. Soc.* **1938,** *60*, 309-319.

55. Newman, C.; Zhou, X.; Goundie, B.; Ghampson, I. T.; Pollack, R. A.; Ross, Z.; Wheeler, M. C.; Meulenberg, R.; Austin, R. N.; Frederick, B. G., Effects of support identity and metal dispersion in supported ruthenium hydrodeoxygenation catalysts. *Appl Catal A Gen* **2014,** *477*, 64-74.
56. Colon, G.; Hidalgo, M. C.; Munuera, G.; Ferino, I.; Cutrufello, M. G.; Navio, J. A., Structural and surface approach to the enhanced photocatalytic activity of sulfated TiO_2 photocatalyst. *Appl Catal B* **2006,** *63*, 45-49.
57. Miroshnichenko, O.; Posysaev, S.; Alatalo, M., A DFT study of the effect of SO_4 groups on the properties of TiO_2 nanoparticles. *Phys. Chem. Chem. Phys.* **2016,** *18* (48), 33068-33076.
58. Miroshnichenko, O.; Posysaev, S.; Alatalo, M., A DFT study of the effect of SO_4 groups on the properties of TiO_2 nanoparticles. *Phys Chem Chem Phys* **2016,** *18*, 33068-33076.
59. Kulkarni, A. P.; Muggli, D. S., The effect of water on the acidity of TiO_2 and sulfated titania. *Appl Catal A* **2006,** *302*, 274-282.
60. Gómez, R.; López, T.; Ortiz-Islas, E.; Navarrete, J.; Sánchez, E.; Tzompanztzi, F.; Bokhimi, X., Effect of sulfation on the photoactivity of TiO_2 sol–gel derived catalysts. *Journal of Molecular Catalysis A: Chemical* **2003,** *193*, 217-226.
61. Znad, H.; Kawase, Y., Synthesis and characterization of S-doped Degussa P25 with application in decolorization of Orange II dye as a model substrate. *J. Mol. Catal. A: Chem.* **2009,** *314*, 55-62.
62. Ohno, T.; Akiyoshi, M.; Umebayashi, T.; Asai, K.; Mitsui, T.; Matsumura, M., Preparation of S-doped TiO_2 photocatalysts and their photocatalytic activities under visible light. . *Applied Catalysis A: General* **2004,** *265* (1), 115-121.
63. Baltrusaitis, J.; Schuttlefield, J.; Zeitler, E.; Grassian, V. H., Carbon dioxide adsorption on oxide nanopartilce surfaces. *Chem. Eng. J.* **2011,** *170*, 471-481.
64. Deiana, C.; Fois, E.; Coluccia, S.; Martra, G., Surface Structure of TiO_2 P25 Nanoparticles: Infrared Study of Hydroxy Groups on Coordinative Defect Sites. *The Journal of Physical Chemistry C* **2010,** *114* (49), 21531-21538.
65. Nanayakka, C. E.; Pettibone, J.; Grassian, V. H., Sulfur dioxide adsorption and photooxidation on isotopically-labeled titanium dioxide surfaces: roles of surface hydroxyl groups and adsorbed water in the formation and stability of adsorbed sulfite and sulfate. *Phys Chem Chem Phys* **2012,** *14*, 6957-6966.
66. Arrouvel, C.; Digne, M.; Breysse, M.; Toulhoat, H.; Raybaud, P., Effects of morphology on surface hydroxyl concentration: a DFT comparison of anatase–TiO_2 and γ-alumina catalytic supports. *Journal of Catalysis* **2004,** *222* (1), 152-166.
67. Saur, P.; Bensitel, M.; Saad, A. B. M.; Lavalley, J. C.; Tripp, C. P.; Morrow, B. A., The Structure and Stability of Sulfated Alumina and Titania. *Journal of Catalysis* **1986,** *99*, 104-110.
68. Mino, L.; Spoto, G.; Ferrari, A. M., CO_2 capture by TiO_2 Anatase Surfaces: A combined DFT and FTIR study. *J. Phys. Chem C* **2014,** *118*, 25016-25026.
69. Mahdavi-Shakib, A.; Arce, J. M.; Austin, R. N.; Schwartz, T. J.; Grabow, L. C.; Frederick, B. G., Use of Surface Hydroxyl Frequencies to Identify the Exposed Facets of Pyrogenic TiO_2 Nanoparticles. **2018,** *(in prep)*.
70. Mahdavi-Shakib, A.; Rahmani-Chokanlu, A.; Schwartz, T. J.; Austin, R. N.; Frederick, B. G., Implications of Electron Scavanging Character of Sulfated Titania for Photochemistry. *(in prep)* **2018**.
71. Omotoso, T. O.; Baek, B.; Grabow, L. C.; Crossley, S. P., Experimental and First-Principles Evidence for Interfacial Activity of Ru/TiO_2 for the Direct Conversion of m-Cresol to Toluene. *ChemCatChem* **2017,** *9* (14), 2642-2651.
72. Boonyasuwat, S.; Omotoso, T.; Resasco, D. E.; Crossley, S. P., Conversion of Guaiacol over Supported Ru Catalysts. *Catal. Lett.* **2013,** *143* (8), 783-791.

73. Liu, Z.; Sriram, V.; Lee, J.-Y., Heterogeneous oxidation of elemental mercury vapor over RuO_2/rutile TiO_2 catalyst for mercury emission control. *Applied Catalysis B Environmental* **2017,** *207*, 143-152.
74. Aranda-Perez, N.; Ruiz, M. P.; Echave, J.; Faria, J., Enhanced Activity and Stability of Ru-TiO_2 for Liquid Phase Ketonization. *Appl Catal A* **2016,** *531*, 106-118.
75. Yang, C.; Zhao, Z.-Y., Investigation of energy band alignments and interfacial properties of rutile NMO_2/TiO_2 (NM = Ru, Rh, Os, and Ir) by first-principles calculations. *Physical Chemistry Chemical Physics* **2017,** *19* (43), 29583-29593.
76. Whittaker, T.; Kumar, K. B. S.; Peterson, C.; Pollock, M. N.; Grabow, L. C.; Chandler, B. D., H_2 Oxidation over Supported Au Nanoparticle Catalysts: Evidence for Heterolytic H_2 Activation at the Metal–Support Interface. *J. Am. Chem. Soc* **2018,** *140*, 16469–16487.
77. Fubini, B.; Bolis, V.; Bailes, M.; Stone, F. S., The reactivity of oxides with water vapor. *Solid State Ionics* **1989,** *32/33* 258-272.
78. Zhao, Z.; Bababrik, R.; Xue, W.; Li, Y.; Briggs, N. M.; Nguyen, D.-T.; Nguyen, U.; Crossley, S. P.; Wang, S.; Wang, B.; Resasco, D. E., Solvent-mediated charge separation drives alternative hydrogenation path of furanics in liquid water. *Nature Catalysis* **2019**.

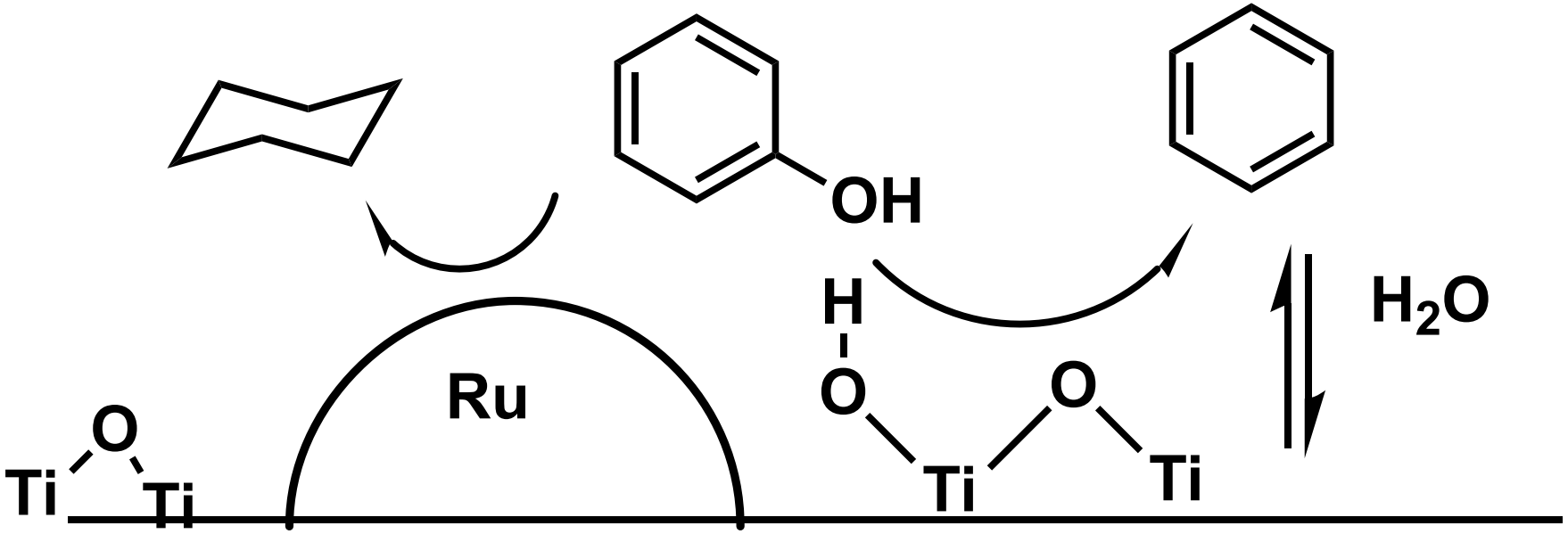

hydrophobic

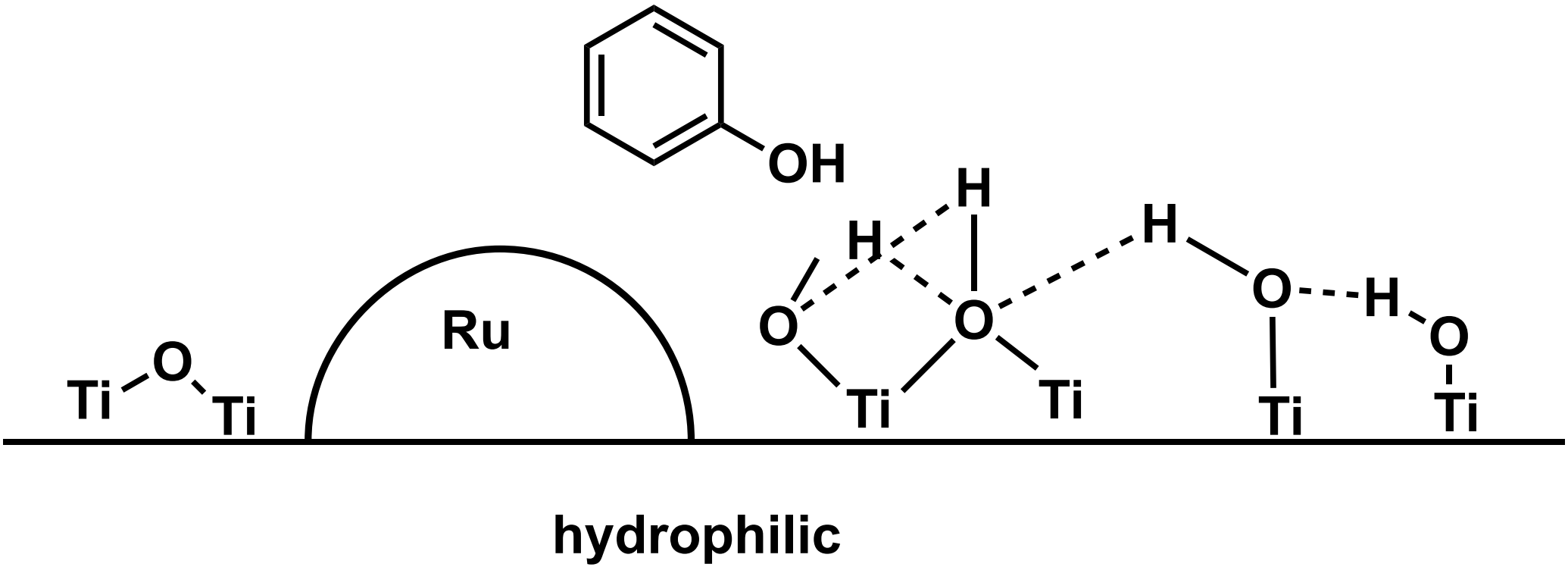

hydrophilic

This work characterized the surface chemistry of a number of different titania samples. All commercial anatase samples were contaminated by sulfur. Hydrogen-bonded surface hydroxyls remained after calcination up to 400 ^{o}C for all anatase samples, in contrast to rutile and the pyrogenic titania materials P25 and P90, in which they were eliminated. Ru(0) catalysts on titania without hydrogen-bonded surface hydroxyls showed enhanced C-O hydrogenolysis selectivity in the presence of water while Ru(0) catalysts on titania with hydrogen-bonded surface hydroxyls showed diminished selectivity in water, suggesting that surface hydrophilicity is important for this reaction.